ELSEVIER

J. Non-Newtonian Fluid Mech. 136 (2006) 118–125

Journal of Non-Newtonian Fluid Mechanics

www.elsevier.com/locate/jnnfm

Matching time dependent pressure driven flows with a Rolie Poly numerical simulation

Rudy Valette [a,*], Malcolm R. Mackley [b], Gabriela Hernandez Fernandez del Castillo [b]

[a] *CEMEF, Ecole des Mines de Paris, UMR-CNRS 7635, B.P. 207, 06904 Sophia-Antipolis, France*
[b] *Department of Chemical Engineering, University of Cambridge, Cambridge CB2 3RA, United Kingdom*

Received 25 November 2005; received in revised form 27 March 2006; accepted 28 March 2006

Abstract

This paper is concerned with pressure driven flow behaviour of molten viscoelastic polymers and reports experimental data and matching numerical simulation for a linear low density polyethylene (LLDPE) melt flowing within an entry and exit slit geometry. Pressure driven processing experiments were carried out using a multipass rheometer (MPR) and time dependent flow birefringence and pressure data were obtained for a series of different flow conditions. A matching numerical simulation was developed using a Rolie Poly constitutive equation with the additional factor of compressibility included. Most but not all rheological parameters were obtained from rheometric viscoelastic measurements on the polymer. Using the non-stretching version of the constitutive equation, the simulation was able to capture many of the observed experimental features and demonstrated that the Rolie Poly equation was effective in describing the flow of the LLDPE tested. The sensitivity of both viscoelasticity and compressibility was demonstrated for the time dependent build up and relaxation of stress and in addition, the simulation was successfully able to predict an initially unexpected time dependent variation of the absolute pressure measured in the upper and lower barrel chambers of the MPR.

Keywords: Multipass rheometer; Rolie Poly model; Row birefringence; Linear low density polyethylene

1. Introduction

The steady development of advanced viscoelastic constitutive equations and their ability to be modelled for complex flow situations using numerical methods has resulted in a situation where numerically modelling is now commonly used to describe and predict complex rheological or engineering processing flows. There is however a need to test both constitutive equation and numerical simulation for non-rheometric flow conditions and this paper presents experimental data and numerical simulation for a flow situation that captures many aspects of pressure driven polymer rheometry and processing.

In terms of polymer melt rheology, the Carreau–Yasuda equation [1] has become a well-established constitutive equation that is capable of describing the shear thinning rheology of molten polymers. In terms of viscoelastic constitutive equations, there has been a progressive evolution from the simple Maxwell model to more advanced equations such as the PTT type model [2] and the Wagner [3] integral model. More recently, the advent of the Doi and Edwards [4] theory has produced a family of molecular based models developed, for example, by Mead et al. [5], Marrucci [6], Wagner et al. [7] and Mcleish and Larson [8]. The Pom-Pom model which was originally formulated for branched polymers has formed the basis of a number of related constitutive equations [9,10] and a development of this type of modelling was the Rolie Poly constitutive equation [11] introduced specifically for linear chains. In this paper, we have chosen to use the Carreau–Yasuda equation to follow shear thinning response alone and the Rolie Poly equation to capture viscoelastic effects.

Recent advances in numerical simulation [12] have made it possible to simulate a wide range of constitutive equations for different complex geometries, see, for example [13]. In the past, a significant difficulty has been associated with the "high Weissenberg number" problem, however the advent of improved numerical techniques, realistic constitutive equations and the application of relaxation spectra rather than single mode, has all helped to make numerical simulation move closer to experimentally observed situations.

In the case of pressure driven flow, Hatzikiriakos and Dealy [14] and subsequently, Durand et al. [15] and Ranganathan et al.

* Corresponding author. Tel.: +33 493957435; fax: +33 492389752.
E-mail address: rudy.valette@ensmp.fr (R. Valette).

0377-0257/$ – see front matter © 2006 Elsevier B.V. All rights reserved.
doi:10.1016/j.jnnfm.2006.03.012

[16] showed that compressibility effects can be important, particularly in relation to time dependent viscoelastic flows and in this paper we introduce constitutive modelling, numerical techniques and compressibility to describe a precise processing situation. The experiments were carried using a Cambridge multipass rheometer (MPR) [17] and this instrument provides well-defined boundary conditions to the flow that can be matched with the numerical simulation. In the experiments reported in this paper, both pressure measurements and flow induced birefringence data are presented and compared with simulation. The coupled, time dependent, birefringence and pressure data provides a strong test for the validity or otherwise of any modelling. Most previously reported matching of simulation with experiment have either involved matching flow birefringence data or pressure drop measurements but not the two simultaneously.

2. Experimental protocol

A Dow linear low density polyethylene LLDPE (Dowlex NG5056E) was used for all experiments. The material is a general purpose extrusion grade polymer that does not have processing difficulties in relation to extrusion instabilities. Experiments were carried out using a slit test section (shown in Fig. 1) with two different multipass rheometers MPR4 and MPR2, the specification for each is given in Table 1. In both cases, polymer pellets were introduced into the MPR barrels and test sections and the system was brought up to the test temperature of 185 °C. In the case of MPR4 experiments, the starting pressure was close to ambient and pressure and flow birefringence data were obtained in a manner similar to that described in ref. [17]. For experiments described in this paper, a single pass extrusion was used where the pistons started from rest and then advanced at a fixed velocity for a set period of time. Flow induced birefringence and pressure values were recorded as a function of time at start up, during and after piston movement. The MPR2 apparatus had larger upstream and downstream volumes than MPR4 and consequently compressibility effects could be more readily

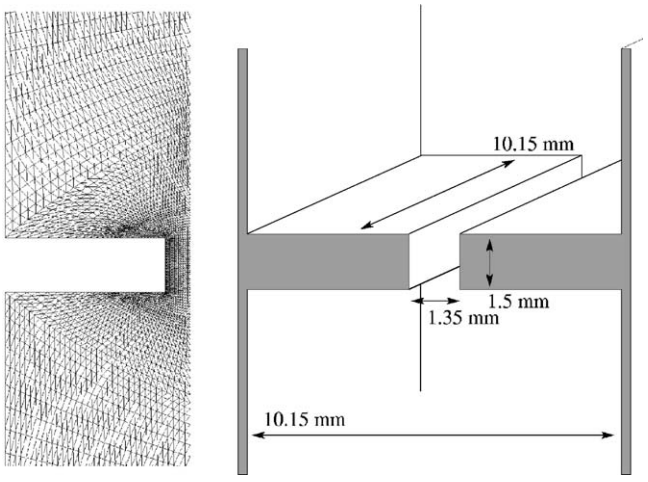

Fig. 1. Detail of the two-dimensional numerical grid and schematic diagram of the slit experimental geometry (gap, $h = 1.35$ mm, length, $L = 1.5$ mm, and width, $W = 10.15$ mm) that was used in both MPR2 and MPR4 experiments.

Table 1
Specification of multipass rheometers 2 and 4, slit geometry and experimental conditions

	MPR4	MPR2
Piston diameter, Φ (mm)	10	12
Sample volume (mm^3)	8735	13562
Mean pressure (bar)	Ambient	20
Piston speed, v_p (mm/s)	5	4
Piston displacement (mm)	10.55	6
Initial upstream volume, V_u (mm^3)	4437	6623
Initial downstream volume, V_d (mm^3)	4277	6918
Slit gap, h (mm)	1.35	1.35
Slit length, L (mm)	1.5	1.5
Slit width, W (mm)	10.15	10.15

followed. In the case of MPR2 experiments, the pistons were initially moved together in order to induce an internal pressure of 20 bar and subsequent experiments were carried out at this mean pressure.

3. Compressibility and constitutive models

The purpose of the modelling approach was to identify both viscoelastic and compressible contributions on the stress dynamic, as these two contributions will involve a time dependent response of the polymer. Three different kinds of models were tested: a compressible viscous (Carreau–Yasuda) model, an incompressible viscoelastic (Rolie Poly) model and a compressible viscoelastic (Rolie Poly) model.

3.1. Compressibility

Isothermal compressible behaviour was simply included in the models using a state law linking thermodynamic pressure and density, assuming that isothermal compressibility K of the polymer is a constant. This then leads to the following state law

$$\frac{\rho}{\rho_{\mathrm{ref}}} = \mathrm{e}^{K(p-p_{\mathrm{ref}})}, \tag{1}$$

where ρ is the density, p the thermodynamic pressure and the subscript 'ref' indicates a reference state.

3.2. Constitutive models

In all the modelling approaches used, the Cauchy stress tensor $\boldsymbol{\sigma}$ was defined as the sum of an isotropic pressure term and a traceless extra-stress tensor $\boldsymbol{\tau}$

$$\boldsymbol{\sigma} = -p\mathbf{I} + \boldsymbol{\tau}. \tag{2}$$

In the case of the compressible Carreau–Yasuda model, $\boldsymbol{\tau}$ is given by

$$\boldsymbol{\tau} = 2\eta(\dot{\gamma}_c)\left(\mathbf{D}(\mathbf{u}) - \frac{\nabla\cdot\mathbf{u}}{3}\mathbf{I}\right), \tag{3}$$

where $\mathbf{u}$ is the velocity field, $\mathbf{D}(\mathbf{u})$ the strain rate tensor and $\eta(\dot{\gamma})$ is the strain rate dependent viscosity classically defined by

$$\eta(\dot{\gamma}_c) = \eta_0(1 + [\lambda\dot{\gamma}_c]^a)^{(n-1)/a}, \tag{4}$$

where a modified expression for the strain rate was used in the compressible case:

$$\dot{\gamma}_c = \sqrt{2\left(\mathbf{D}(\mathbf{u}) - \frac{\nabla\cdot\mathbf{u}}{3}\mathbf{I}\right) : \left(\mathbf{D}(\mathbf{u}) - \frac{\nabla\cdot\mathbf{u}}{3}\mathbf{I}\right)}. \quad (5)$$

In the case of the Rolie Poly model, which is a suitable model for linear polymers, proposed by Likhtman and Graham [11], we choose a non-stretching version, assuming that chain stretch was not activated for the moderate values of the srain rate and relaxation times present in our experiments. A multimode version was used where the extra-stress tensor $\boldsymbol{\tau}$ is then expressed by

$$\boldsymbol{\tau} = \sum_i 3G_i\left(\mathbf{C}_i - \frac{1}{3}\mathbf{I}\right), \quad (6)$$

where G_i is the shear modulus and $\mathbf{C}_i$ the "orientation" tensor (a unity trace conformation tensor) of the ith mode, and the evolution equation for $\mathbf{C}_i$ is given by

$$\frac{d\mathbf{C}_i}{dt} - \nabla\mathbf{u}\cdot\mathbf{C}_i - \mathbf{C}_i\cdot\nabla^t\mathbf{u} + 2(\nabla\mathbf{u} : \mathbf{C}_i)\mathbf{C}_i = -\left(\frac{1}{\theta_i} + 2\beta|\nabla\mathbf{u} : \mathbf{C}_i|\right)\left(\mathbf{C}_i - \frac{1}{3}\mathbf{I}\right), \quad (7)$$

where θ_i is a relaxation time and β is the convective constrain release parameter. As suggested by Ianniruberto and Marrucci [18], we modified the original equation by adding an absolute value to the convective term $|\nabla\mathbf{u}{:}\mathbf{C}_i|$ in order to account for orientation renewal occurring in fast reversing flows (which is encountered in our case at slit outlet). Moreover, this modification avoids the appearance of numerical instabilities due to possible change of sign of the overall time $((1/\theta_i) + 2\beta(\nabla\mathbf{u}{:}\mathbf{C}_i))$ of the relaxation term in Eq. (7).

A weak coupling between compressible effects and viscous/viscoelastic effects was chosen, by assuming a linear density dependence of the Carreau–Yasuda plateau viscosity η_0 and viscoelastic shear modulus G_i, see, for example, Wapperom and Hulsen [19]:

$$\eta_0 = \frac{\rho}{\rho_{ref}}\eta_{0_{ref}}, \quad (8)$$

$$G_i = \frac{\rho}{\rho_{ref}}G_{i_{ref}}. \quad (9)$$

Influence of density on other material parameters is neglected. By choosing a model involving a weak coupling, we assumed that the underlying kinetic theory on which the Rolie Poly is based is not affected by compressibility, whereas the expression of the viscoelastic shear modulus is proportional to the density as it is usually shown in the so called microscopic expression for the stress tensor [4].

3.3. Parameter identification

A six-mode linear relaxation spectrum was determined from linear dynamic moduli measurements using a ARES Rheometrics rheometer (see Table 2). Assuming the validity of the Cox–Merz rule, one then obtains the steady shear viscosity as a function of shear rate $\eta(\dot{\gamma})$, which was used to determine the Carreau–Yasuda parameters (see Table 2).

The CCR β parameter of Eq. (7) does not significantly influence the $\eta(\dot{\gamma})$ curve, the pressure difference or the time dependent response of the direct simulation. We have therefore chosen to use a semi-arbitrary identification procedure by adjusting its influence and matching between numerical and MPR4 experimental birefringence pattern observed at slit outlet. The value of $\beta = 0.2$ gave good qualitative results and was then chosen for all simulations.

Finally, the isothermal compressibility parameter K was simply experimentally measured by moving both MPR pistons together and fitting the pressure—ln(volume) experimental data. This procedure gave a value of $1.26 \times 10^{-9}\,\mathrm{Pa}^{-1}$ for K.

3.4. Characteristic time scales for the experiments

The apparent shear rate of the steady-state flow within the slit is classically defined as

$$\dot{\gamma}_a = \frac{\pi\Phi^2 v_p}{4h^2 W}, \quad (10)$$

where Φ and v_p are, respectively, the piston diameter and the piston speed and h and W are, respectively, the slit gap and width. It is then possible to define a Weissenberg number of the flow

Table 2
Carreau–Yasuda parameters and linear viscoelasticity spectrum (half of the shortest relaxation mode has been splitted into a Newtonian solvent contribution) at 185 °C

Carreau–Yasuda model						
η_0 (Pa s)						8.584×10^3
λ (s)						6.401×10^{-2}
a						5.151×10^{-1}
n						3.605×10^{-1}
	Mode[a]					
	1	2	3	4	5	6
G_i (Pa)	$0.5 \times 7.69 \times 10^5$	1.82×10^5	7.67×10^4	2.03×10^4	3.53×10^3	5.12×10^2
θ_i (s)	6.56×10^{-4}	3.65×10^{-3}	2.03×10^{-2}	1.13×10^{-1}	6.27×10^{-1}	3.49

[a] Six modes relaxation times spectrum.

by using the viscosity averaged relaxation time of the material

$$We = \dot{\gamma}_a \times \sum_i \frac{G_i \theta_i^2}{G_i \theta_i}, \tag{11}$$

however it should be remembered that the long relaxation modes are dominant in relation to viscoelastic effects.

To evaluate a time scale for compressible effects within the multipass rheometer, the same modelling assumptions as in ref. [16] have been used, considering that compressible effects are mainly located in the upstream and downstream barrels and that pressure gradient is created by the flow within the slit. It results in the following differential equation for the pressure drop

$$\frac{d\Delta p}{dt} = \frac{1}{K} \times \left(\frac{1}{V_u} + \frac{1}{V_d} \right) \times \left(\pi \frac{\Phi^2}{4} v_p - Q_s \right), \tag{12}$$

where V_u and V_d are characteristic volumes of, respectively, the upstream and downstream barrels and Q_s is the flow rate within the slit. For a given pressure drop, the value of Q_s is estimated by the equivalent steady-state Newtonian formula

$$Q_s = \frac{h^3 W}{12 \eta_a L} \Delta p, \tag{13}$$

where η_a is the Carreau–Yasuda viscosity (Eq. (4)) calculated for $\dot{\gamma}$ equal to $\dot{\gamma}_a$ and L is the slit length. Substituting this value in Eq. (11) gives a first-order differential equation for the pressure drop, with the following characteristic time scale for compressible effects:

$$\theta_{comp} = \frac{12 \eta_a L K}{h^3 W} \left(\frac{1}{V_u} + \frac{1}{V_d} \right)^{-1}. \tag{14}$$

Using the values given in Tables 1 and 2 for MPR4 experiments gives the following values for, respectively, the apparent shear rate, the Weissenberg number and the characteristic time scale for compressible effects: 21.2 s^{-1}, 18.6 and 6.5×10^{-3} s. For MPR2 experiments, they, respectively, are: 24.5 s^{-1}, 21.5 and 9.6×10^{-3} s.

4. Numerical simulation

A two-dimensional, time dependent, finite element code, based on the MEF++ software (developed at the GIREF, Université Laval, Que., Canada, see, for example, Belhamadia et al. [20]) was used to simulate the flow of the polymer within the multipass rheometer.

The numerical method uses an extension of incompressible mixed finite elements and a low Mach number compressible flow solver, see comprehensive work of Webster and co-workers [21–23]. The code is based on a decoupling, within each time step of an implicit Euler integration technique, between the compressible Stokes problem perturbed by a viscoelastic contribution and the evolution equations for the conformation tensor of each mode, stabilized by a streamline upwind Petrov/Galerkin method, see Ervin and Miles [24] for a complete analysis of the numerical strategy.

The mixed weak formulation of the compressible Stokes problem, in which inertia effects were neglected, was classically expressed by taking the L_2-inner product $\langle .,. \rangle$ on the computational domain of both momentum and mass conservation equations with admissible test functions:

$$\left\langle 2\eta_s \left(\mathbf{D}(\mathbf{u}) - \frac{\nabla \cdot \mathbf{u}}{3} \mathbf{I} \right), \mathbf{D}(\mathbf{u}^*) \right\rangle - \langle p, \nabla \cdot \mathbf{u}^* \rangle = - \left\langle \sum_i \boldsymbol{\tau}_i, \mathbf{D}(\mathbf{u}^*) \right\rangle \tag{15}$$

$$\left\langle K \left(\frac{\partial p}{\partial t} + \mathbf{u} \cdot \nabla p \right) + \nabla \mathbf{u}, p^* \right\rangle = 0, \tag{16}$$

where the viscous term η_s in the Stokes problem was obtained by splitting half of the shortest viscoelastic mode of the Rolie Poly model into a solvent Newtonian behaviour of viscosity $\eta_s = 0.5 \times G_1 \times \theta_1$. Each viscoelastic mode contributed to the stress as given in Eq. (6) and the SUPG formulation for each conformation tensor evolution equation was:

$$\left\langle \frac{d\mathbf{C}}{dt} - \nabla \mathbf{u} \cdot \mathbf{C} - \mathbf{C} \cdot \nabla^t \mathbf{u} + 2(\nabla \mathbf{u} : \mathbf{C})\mathbf{C} + \left(\frac{1}{\theta} + 2\beta |\nabla \mathbf{u} : \mathbf{C}| \right) \times \left(\mathbf{C} - \frac{1}{3} \mathbf{I} \right), \mathbf{C}^* + h \frac{\mathbf{u}}{|\mathbf{u}|} \cdot \nabla \mathbf{C}^* \right\rangle, \tag{17}$$

where h is the square root of the surface of the element.

The domain was divided into triangle elements (see Fig. 1) and spatial discretization was performed using a quadratic approximation for the velocity and linear approximation for the pressure and conformation tensor [24]. Finally, using a "quasi-Newton" scheme, the weak forms of the Stokes and constitutive equations problems were linearized (apart from the CCR term in Eq. (17) which involves an absolute value) and non-symmetrical algebraic systems were solved by using a direct solver.

5. Results

Experimental results are either presented in terms of flow birefringence retardation contours or pressure data as a function of time. Matching numerical simulations were performed for the same volumetric flow boundary conditions using the rheological data provided in Table 2.

Numerical computations were done on a mesh made of 5641 elements (of which a detail is shown in Fig. 1), which corresponds to 15 elements in the slit gap, and by using a time step of 10^{-4} s. For each computation, upstream and downstream volumes of the mesh are the same as given in Table 1. Accuracy of computed solutions has been checked by comparing pressure curves and birefringence patterns obtained on a coarser mesh made of 2807 elements (10 elements in slit gap) and by using a time step of 5×10^{-4} s.

A range of stress optical coefficients have been specified for polyethylene [25] and we have chosen a value of 1.43×10^{-9} Pa^{-1} that falls within the range quoted for LLDPE and gives consistent results with our observations. It should be remembered that the numerical simulation is two-dimensional

and the birefringence is calculated on the assumption that the retardation is uniform throughout the depth of the slit. Both these assumptions are not true, however recent numerical results by Clemeur et al. [26] show that the two-dimensional approximation for flows such as this is not unreasonable.

5.1. Comparison between flow induced birefringence and numerical simulation, MPR4 experiments

A series of time dependent flow birefringence patterns and matching numerical principle stress difference contours are shown in Fig. 2. For this set of data, the simulation used the Rolie Poly constitutive equation coupled with compressible flow. The top section of each time sequence corresponds to the numerical simulation and the bottom section to the experimental flow birefringence. The piston movement starts at $t = 0$ s and stops at $t = 2.81$ s. The photographs and simulation show good qualitative matching although close inspection shows some quantitative differences. At time $t = 0.06$ s, the general form of the contours are similar, but the centre line contours in the entry region do not match exactly. The steady flow situation is captured at times $t = 0.84$ and 1.2 s and again the entry flow match is poorer than the slit or exit flow. Relaxation behaviour after piston movement cessation is followed for times $t = 2.85$–3.4 s and here the simulation is predicting a slightly faster relaxation than experimentally observed.

Given the uncertainties in both the experiments and the numerical simulation, the overall impression from the data given in Fig. 2 is that the model predictions are satisfactory. Exact quantitative comparison of flow birefringence patterns is possible but difficult [27] and we have found in this case that a detailed comparison of pressure behaviour is more useful when comparing different aspects of the numerical simulation and this is given in the two following sections.

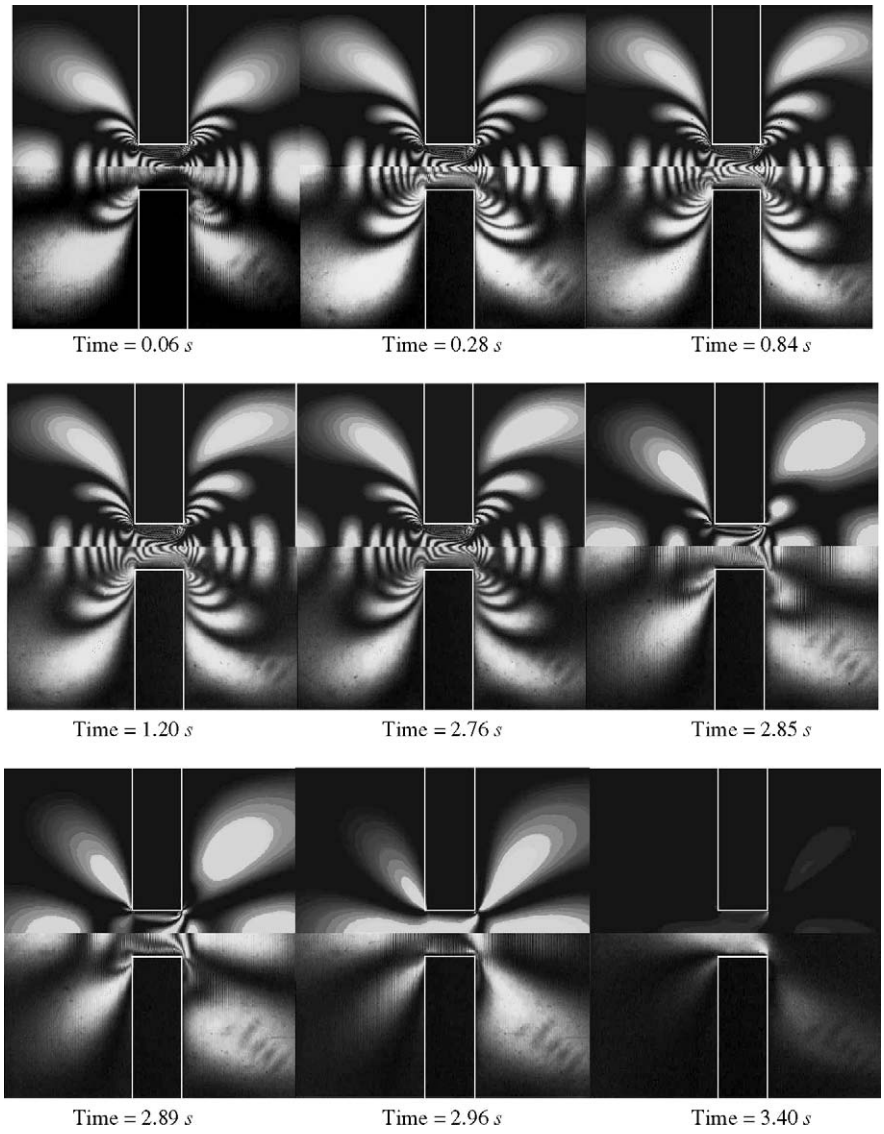

Fig. 2. MPR4, matching of time dependent simulation (top) with experiment (bottom) for LLDPE at 185 °C for a piston speed of 5 mm/s. Flow is from left to right in the figure, slit geometry is drawn in white on the pictures. Rolie Poly simulation with compressible flow.

5.2. The effect of compressibility and viscoelasticity on pressure difference behaviour, MPR4 experiments

The detailed way in which different simulations compare with pressure difference measurement is shown in Fig. 3. The experimental data shows the classic pressure build up, followed by a steady flow period and a subsequent stress decay. The pressure data in Fig. 2 corresponds to same experimental birefringence sequence given in Fig. 2. Three simulation profiles are shown and in general all the simulations capture the gross features of the pressure profile however there are differences particularly in the time dependent part of the profiles. The compressible flow Carreau equation captures the time dependent pressure build up well, but gives a low steady-state pressure. The steady-state mismatch is probably due to a lack of the model predicting die entry and exit effects and should not necessarily be considered as a major failing of the model. The compressible Carreau pressure relaxation data on flow cessation is interesting in that at high pressures the model initially follows the experimental data well; however, after longer times, the experimentally observed pressure relaxation is slower than predicted. The incompressible Rolie Poly simulation had as expected a faster pressure build up. The steady flow match was improved over the Carreau and the initial pressure relaxation is also faster than the Carreau.

The compressible Rolie Poly simulation gave an accurate match throughout the simulation. Pressure build up and steady flow were in good agreement with experiment and, of particular interest, both short and long time pressure relaxation were well matched. It can be concluded from these results that for this set of conditions, the early stages of pressure release is controlled by compressibility effects and the later stages by viscoelasticity. The data presented in both Figs. 2 and 3 show that the compressible flow Rolie Poly has matched the experimental data to a tolerance level associated with the experimental uncertainties.

For the experimental conditions described here, the effect of compressibility and viscoelasticity were relatively mild and in order to demonstrate stronger compressibility effects, further

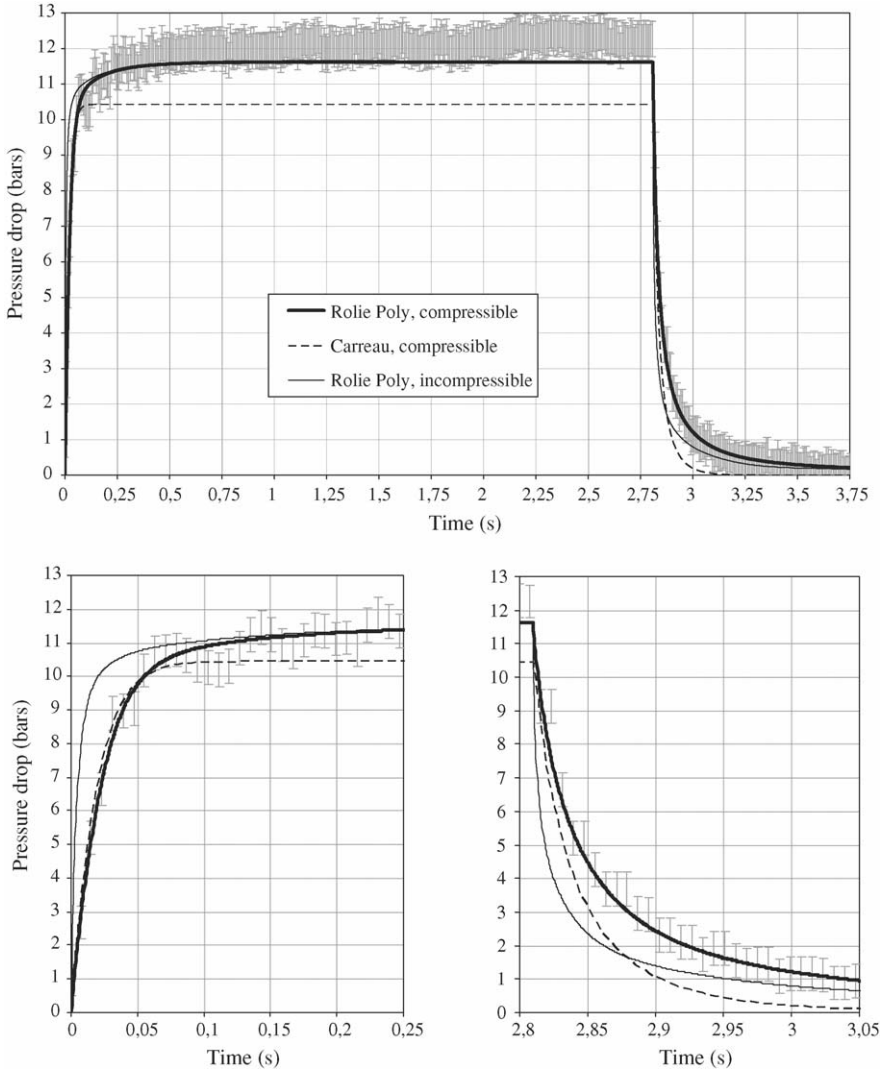

Fig. 3. Time dependent pressure difference profile for MPR4, LLDPE at 185 °C at a piston speed of 5 mm/s, complete curve (top) and details of start up (bottom left) and relaxation (bottom right) flow. Experimental data (error bar I), compressible Carreau (– – –), incompressible Rolie Poly (—) and compressible Rolie Poly (▬).

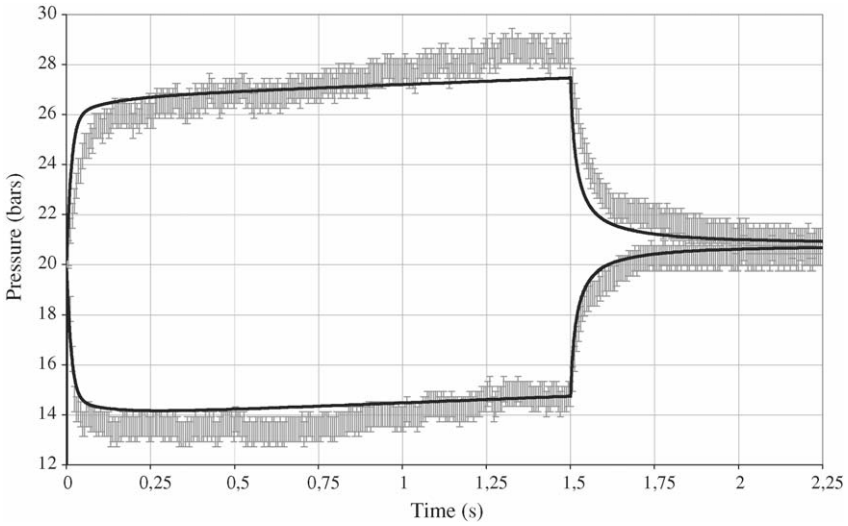

Fig. 4. Time dependent absolute pressure profiles for MPR2, LLDPE at 185 °C at a piston speed of 4 mm/s. Experimental data (error bar I) for both top (top curves) and bottom (bottom curves) piston, matching numerical simulation (▬) for compressible Rolie Poly model.

experiments using the larger volume MPR2 were carried out as described in the next section.

5.3. The effect of absolute pressure on pressure profiles, MPR2 experiments

A second series of experiments using the same grade polymer and the same slit section as used in the previous section was carried out with MPR2. In this case, the polymer was pre pressurised to 20 bars and the flow carried out at this mean pressure. For the ambient pressure MPR4 experiments described in the previous section, the only way that the pressure could change during flow was for the pressure in the upstream chamber to increase. In the case of the pre pressurised MPR2 experiments, the situation is different because with the onset of flow, both the upstream and downstream pressure can change.

Fig. 4 shows an experimental example of the way in which both the upstream and downstream absolute pressure changes. With the onset of piston movement it can be seen that the upstream pressure increases and the downstream pressure decreases. The system approaches a near steady-state where the pressure difference (not shown) is a constant but both upstream and downstream pressures are slowly increasing. On flow cessation, both pressures relax towards the no flow value.

A compressible Rolie Poly simulation is also shown in Fig. 4 and the match between experimental data and simulation is in reasonably good agreement. The simulation captures the distribution of pressure between the top and bottom barrels and matches, in particular, the pressure relaxation process of the system.

6. Conclusions and discussion

In this paper, time dependent flow birefringence and pressure profile data has been presented that provides a basis for testing constitutive equations and also numerical schemes. In work reported here, a non-Newtonian "Carreau" constitutive equation and a viscoelastic "Rolie Poly" constitutive equation has been tested. In addition, the effect of compressibility has been explored both in relation to birefringence and pressure evolution.

The LLDPE pressure build up, steady flow and stress relaxation reported in this paper provided a useful dataset for detailed simulation matching and in general the compressible flow, viscoelastic Rolie Poly numerical simulation was found to match the data. The results show that both pressure and flowbirengence data can be matched with simulation for the same experimental situation. Compressibility has been included within the simulation and for the situation studied here, compressibility was found to have a mild, but quantitative effect that improves the matching of data. The simulation has also been able to predict the absolute pressure behaviour of pressure within both the barrels of the MPR and this assists the understanding of the way this rheometer operates. This paper has considered only a limited set of conditions for one particular polymer and it can be expected that other polymers with broader viscoelastic relaxation spectra will show stronger effects for viscoelasticity. Equally flow situations where pressure are higher and volumes greater will show enhanced compressibility effects.

Acknowledgements

We would like to thank Professor J.-F. Agassant for encouraging collaboration between CEMEF and Cambridge University and enabling RV to spend 1 year at Cambridge. GH would like to thank CONACyT for financial support and RV would like to thank Prof. A. Fortin and the GIREF staff for their continuous support, advice and providing the MEF++ finite element software.

References

[1] K. Yasuda, R.C. Armstrong, R.E. Cohen, Shear flow properties of concentrated solutions of linear and star branched polystyrenes, Rheol. Acta 20 (1981) 163.

[2] N. Phan-Thien, R.I. Tanner, A new constitutive equation derived from network theory, J. Non-Newtonian Fluid Mech. 2 (1977) 353.
[3] M.H. Wagner, Analysis of time dependent stress growth data for shear and elongational flow of a low density polyethylene, Rheol. Acta 18 (1979) 33.
[4] M. Doi, S.F. Edwards, The Theory of Polymer Dynamics, Oxford University Press, New York, 1986.
[5] D.W. Mead, R.G. Larson, M. Doi, A molecular theory for fast flows of entangled polymers, Macromolecules 31 (1998) 7895.
[6] G. Marrucci, Dynamics of entanglements: a nonlinear model consistent with the Cox–Merz rule, J. Non-Newtonian Fluid Mech. 62 (1996) 279.
[7] M.H. Wagner, P. Rubio, H. Bastian, The molecular stress function model for polydisperse polymer melts with dissipative convective constraint release, J. Rheol. 45 (2001) 1387.
[8] T.C.B. McLeish, R.C. Larson, Molecular constitutive equations for a class of branched polymers: the Pom-Pom polymer, J. Rheol. 42 (1998) 81.
[9] T.C.B. Mcleish, J. Allgaier, D.K. Bick, G. Bishko, P. Biswas, R. Blackwell, B. Blottiere, N. Clarke, B. Gibbs, D.J. Groves, A. Hakiki, R.K. Heenan, J.M. Johnson, R. Kant, D.J. Read, R.N. Young, Dynamics of entangled H-polymers: theory, rheology, and neutron-scattering, Macromolecules 32 (1999) 6734.
[10] R.J. Blackwell, T.C.B. McLeish, O.G. Harlen, Molecular drag strain coupling in branched polymer melts, J. Rheol. 44 (2000) 121.
[11] A.E. Likhtman, R.S. Graham, Simple constitutive equation for linear polymer melts derived from molecular theory: Rolie-Poly equation, J. Non-Newtonian Fluid Mech. 114 (2003) 1.
[12] F.P.T. Baaijens, M.A. Hulsen, P.D. Anderson, The Use of Mixed Finite Element Methods for Viscoelastic Fluid Flow Analysis, Encyclopedia of Computational Mechanic, vol. 3 Fluids, John Wiley & Sons, 2004, pp. 481–498.
[13] W.M.H. Verbeeten, G.W.M. Peters, F.P.T. Baaijens, Differential constitutive equations for polymer melts: the extended Pom-Pom model, J. Rheol. 45 (2001) 823.
[14] S.G. Hatzikiriakos, J.M. Dealy, Start up transients in a capillary rheometer, Polym. Eng. Sci. 34 (1994) 493.
[15] V.B. Durand, B. Vergnes, J.-F. Agassant, E. Benoit, R.J. Koopmans, Experimental study and modelling of oscillatory flow in high density polyethylene, J. Rheol. 40 (1996) 383.
[16] M. Ranganathan, M.R. Mackley, P.H.J. Spittler, Experimental observations and modelling of time dependent capillary flow for a high density polyethylene using a multipass rheometer, J. Rheol. 43 (1999) 443.
[17] K. Lee, M.R. Mackley, The application of the multi-pass rheometer for precise rheo-optic characterisation of polyethylene melts, Chem. Eng. Sci. 56 (2001) 5653.
[18] G. Ianniruberto, G. Marrucci, A simple constitutive equation for entangled polymers with chain stretch, J. Rheol. 45 (2001) 1305.
[19] P. Wapperom, M.A. Hulsen, Thermodynamics of viscoelastic fluids: the temperature equation, J. Rheol. 42 (1998) 999.
[20] Y. Belhamadia, A. Fortin, E. Chamberland, Anisotropic mesh adaptation for the solution of the Stefan problem, J. Comput. Phys. 194 (2004) 233.
[21] I.J. Keshtiban, F. Belblidia, M.F. Webster, Numerical simulation of compressible viscoelastic liquids, J. Non-Newtonian Fluid Mech. 122 (2004) 131.
[22] M.F. Webster, I.J. Keshtiban, F. Belblidia, Computation of weakly compressible highly-viscous liquid flows, Eng. Comput. 21 (2004) 777.
[23] I.J. Keshtiban, F. Belblidia, M.F. Webster, Computation of incompressible and weakly-compressible viscoelastic liquids flow: finite element/volume schemes, J. Non-Newtonian Fluid Mech. 126 (2005) 123.
[24] V.J. Ervin, W.W. Miles, Approximation of time-dependent viscoelastic fluid flow: SUPG approximation, SIAM J. Numer. Anal. 41 (2003) 457.
[25] K. Lee, M.R. Mackley, The significance of slip in matching polyethylene processing data with numerical simulation, J. Non-Newtonian Fluid Mech. 94 (2000) 159.
[26] N. Clemeur, R.P.G. Rutgers, B. Debbaut, Numerical evaluation of three-dimensional effects in planar flow birefringence, J. Non-Newtonian Fluid Mech. 123 (2004) 105.
[27] J.-F. Agassant, F. Baaijens, H. Bastian, A. Bernnat, A.C.B. Bogaerds, T. Coupez, B. Debbaut, A.L. Gavrus, A. Goublomme, M. van Gurp, R.J. Koopmans, H.M. Laun, K. Lee, O.H. Nouatin, M.R. Mackley, G.W.M. Peters, G. Rekers, W.M.H. Verbeeten, B. Vergnes, M.H. Wagner, E. Wassner, W.F. Zoetelief, The matching of experimental polymer processing flows to numerical simulation, Int. Polym. Proc. 17 (2002) 3.